Dynamics and Control of a Maglev Vehicle

W. Ko, Q. Han, and C. Ham
University of Central Florida
Orlando, FL 32816, U.S.A.

ABSTRACT

In this paper, dynamics of a Maglev vehicle was analyzed and controls utilizing an optimized damping and an LQR algorithms were designed to stabilize the vehicle. The dynamics of magnetically levitated and propelled Maglev vehicle are complex and inherently unstable. Moreover, 6-DOF system dynamics is highly nonlinear and coupled. The proposed control schemes provide the dynamic stability and controllability, which computer simulations confirmed the effectiveness.

Keywords: Maglev, stability, damping control, LQR control, Halbach array, levitation, 6-DOF.

1. INTRODUCTION

Maglev has been identified as a ground-based technology with the potential to be a major component in the launch system for the next generation of space transport vehicles. The operational principal is that the space vehicle mounted on a carriage is accelerated on a track using electric power until it reaches a predetermined design speed. When this velocity is reached, the vehicle's main engines are started and the vehicle is released from the carriage to continue to orbit under its own power. The main advantage is that the initial velocity is obtained using a source of energy external to the vehicle, which enables a savings of over 20% in onboard fuel [1]. Also by using a horizontal take-off versus a vertical take-off, further cost advantages can be realized through the reduction of the required thrust to weight ratio [2]. The reference system used for this paper is the repulsive-force maglev track developed by the Lawrence Livermore National Laboratory, Inductrack. The unique feature of the Inductrack is the use of a special arrangement of magnets called the Halbach array. The magnetic orientation provides the magnetic field lines to combine and form a concentrated sinusoidal field below the array. It also causes the field above the array to cancel out.

By using rare earth magnets and the Halbach array, the weight of the magnets is only about 2% of the levitated weight [3]. A moving carriage has special arrays of permanent magnets mounted on its inside surface. Relative motion between these magnets and the coils in the track induces a current in the track coils. These currents interact with the horizontal magnetic field from the arrays and cause the carriage to be levitated above the track. The carriage is propelled down the track by pulsed currents in the drive coils, synchronized with the position of the carriage. These pulses interact on the vertical magnetic fields from the magnets. As showed in Figure 2, the unique structural feature of the Inductrack is that there are magnets mounted on the carriage to act on the underside of the track as well as the top. These are mounted on each side at a 45° angle. These enhance the stability of the carriage in both the vertical and lateral directions. While this geometric configuration does increase the critical speed for levitation, the enhanced stability provided is worth the penalty. Even with these additional magnet arrays there still are some stability problems during the initial levitation phase [4].

2. 6 DOF VEHICLE DYNAMICS

The focus of this analysis is the portion of the acceleration after the carriage is levitated and free from the auxiliary guide wheels. This analysis assumes the basic geometry of the LLNL carriage as defined in the final report [3].

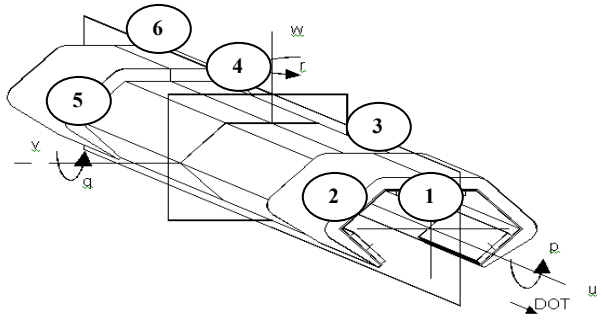

Figure 1. Carriage Axis Arrangement

Equations of Motion

The coordinate system for the inertial reference frame is defined with the x-axis in the horizontal direction of travel, the y-axis lateral across the track and the z-axis in the vertical direction. The orientation of the three linear velocities u, v and w and three rotation velocities p, q and r are shown in Fig. 1. Then, the six degree of freedom equations for the motion of a rigid body are [6, 7]:

$$\mathbf{f}_o = m\left(\left(\frac{\partial \mathbf{v}_o}{\partial t}\right)_{rel} + \boldsymbol{\omega} \times \mathbf{v}_o + \dot{\boldsymbol{\omega}} \times \mathbf{r}_G + \boldsymbol{\omega} \times (\boldsymbol{\omega} \times \mathbf{r}_G)\right) \quad (1)$$

$$\mathbf{m}_o = \mathbf{I}_o \dot{\boldsymbol{\omega}} + \boldsymbol{\omega} \times (\mathbf{I}_o \boldsymbol{\omega}) + m\mathbf{r}_G \times \left(\left(\frac{\partial \mathbf{v}_o}{\partial t}\right)_{rel} + \boldsymbol{\omega} \times \mathbf{v}_o\right) \quad (2)$$

where, f_0 is force, m is mass, v_0 is velocity, w_0 is the total angular velocity, m_0 is moment, I_o is the inertial tensor as defined at the origin of the carriage-fixed coordinate system, and r_G is the vector from the inertial frame to the carriage center of gravity.

Levitation Force

For convenience of discussion, the force perpendicular to the surface of the array will be referred to as the levitation force.

The levitation force produced per circuit by the magnet array is given by [5]:

$$F = \frac{B_0^2 w^2}{2kL} \frac{1}{1+(R/\omega L)^2} \exp(-2ky_1) \quad \text{Newton} \tag{3}$$

where:
R is the resistance of the circuit.
w is the transverse width of each array.
y_1 is the distance from the array to the coils.
ω is the excitation frequency of the circuit and is given by the relationship $\omega=kv$.
v is the array velocity as it passes over the coils (m/s).
k is given by the relationship $k=2\pi/\lambda$, where λ is the array wavelength (0.1m).
L is the inductance of the circuit, and is given by[3, 5]:
and B_0 is the peak field at the surface of the array and is defined as[5]:

$$B_0 = B_r[1-\exp(-kd)] \frac{\sin(\pi/M)}{(\pi/M)} \quad \text{Tesla} \tag{4}$$

where d is the thickness in the vertical direction of the Halbach array and M is the number of magnet elements per wavelength

Levitation dynamics
For the vehicle levitated above the track coils, the magnetic levitation force ***F*** is a function of the distance between the magnetic array and levitation coils, ***d***. The force can be expanded in a Taylor series in the perturbed small displacement variables about the equilibrium- nominal position [8].

$$F(d) = F(d_0) + \frac{\partial F}{\partial d}|_{d=d_0} (d - d_0) \tag{5}$$

and $F(d_0)=mg$, m is the mass of the vehicle, and g is the gravity acceleration rate of earth.

$$F_L = \frac{B_0^2 w^2}{2kL} \frac{1}{1+(R/\omega L)^2} \exp(-2k\Delta z) = F(d_0)(1-2k\Delta d) \tag{6}$$

and it follows from the equation of motion

$$m\ddot{\Delta d} = -F(d_0)2k\Delta d = -mg2k\Delta d \tag{7}$$

Equilibrium condition
The designed nominal levitation height for this track is 1.5 cm. At this height the forces from the three magnet arrays will be in equilibrium. Perturbations from the design height will increase the force between the array and the track on the surfaces that are closer, and reduce the force on the arrays that are farther away, resulting in a centering force on the carriage. These forces are combined as follows based on the geometry of the carriage, and the physical properties for the magnets:

Vertical translation:

$$\sum F_z = F_{z_3} - F_{z_1} - F_{z_2} + F_{z_6} - F_{z_4} - F_{z_5} \tag{8}$$

Lateral translation:

$$\sum F_y = F_{y_1} - F_{y_2} + F_{y_4} - F_{y_5} \tag{9}$$

Roll:

$$\Sigma M_x = .119(F_{y_1} - F_{y_2} + F_{y_4} - F_{y_5}) \tag{10}$$

Pitch:

$$\Sigma M_z = .26(F_{z_3} - F_{z_1} - F_{z_2} + F_{z_6} - F_{z_4} - F_{z_5}) \tag{11}$$

Yaw:

$$\Sigma M_y = .26(F_{y_1} - F_{y_2} - F_{y_4} + F_{y_5}) \tag{12}$$

Above analysis is based on the equilibrium position. Following the system static stiffens is analyzed for lateral, roll, pitch, and yaw directions [9].

Lateral
Consider the vehicle is in a non-equilibrium position with displacement Δy. The offset is +Δy for array 1 and 4, and -Δy for array 2 and 5 laterally. The lateral arrays will generate the lateral restoration force, from (3) and (9)

$$\sum F_{unbncd\_y} = 2\frac{B_0^2 w^2}{2kL} \frac{1}{1+(R/\omega L)^2} [\exp(-2k(y_1-\Delta y) - \exp(-2k(y_1+\Delta y))] \approx 8F_{bncd\_y} k\Delta y \tag{13}$$

where, F_{bncd_y} is a each magnet force when equilibrium position. The lateral stiffness is

$$\frac{\partial (F_{unbncd\_y})}{\partial(\Delta y)} = 8F_{bncd\_y} k$$

This means that the lateral restoration force will always increase as the lateral displacement increases.

Roll
The lateral array will generated restore force, the related position change is $\Delta y \cong L_z \sin(\phi) = \phi L_z$.
where, L_z is the lateral array center to the center of the vehicle in the z direction.

$$F_{right\_unbncd} = F_{y_1} + F_{y_4} = 2\frac{B_0^2 w^2}{2kL} \frac{1}{1+(R/\omega L)^2} \exp(-2k(y_1-\Delta y)) \approx 2F_{bncd\_y} \times \left[1 + 2kL_z\phi + 2(kL_z)^2\phi^2\right] \tag{14}$$

Applying same equation to the left lower magnet, then we get total roll moment

$$T_{roll\_unbncd} = 8F_{bncd\_y} kL_z^2 \phi$$

The roll stiffness is

$$\frac{\partial(T_{roll\_unbncd})}{\partial(\phi)} = 8F_{bncd\_y}kL_z{}^2$$

This means that the roll restoring moment also increases as the roll displacement increases.

Pitch

If the levitation array pair is in a non-equilibrium position with displacement -Δz for front array 1, 2 and 3, +Δz for array 4, 5 and 6; and L_x is the distance between center of each levitation array and the center of the vehicle in *x* direction; the pitch angle $\theta \approx \Delta z / L_x$. If θ is very small, we can neglect the higher order items.

$$\begin{aligned} &< F_{front\_unbncd} >= F_{z_3} - F_{z_1} - F_{z_2} \\ &= \frac{B_0^2 w^2}{2kL} \frac{1}{1+(R/\omega L)^2} \exp(-2k(z-\Delta z)) \\ &\quad - 2\frac{B_0^2 w^2}{2kL} \frac{1}{1+(R/\omega L)^2} \exp(-2k(z+\Delta z)) \\ &\approx 0.06 \cdot F_{z_3} \cdot \left[1 + 2kL_x\theta + 2(kL_x)^2\theta^2\right] \end{aligned} \tag{15}$$

Applying to same equation to rear magnet, then we get

$$0.06 \cdot F_{z_6} \cdot \left[1 - 2kL_x\theta + 2(kL_x)^2\theta^2\right]$$

$$T_{pitch\_unbncd} = 0.12F_{bncd\_upper} \cdot kL_x{}^2\theta$$

The pitch stiffness,

$$\frac{\partial(T_{pitch\_unbncd})}{\partial(\theta)} = 0.12F_{bncd\_upper} \cdot kL_x{}^2$$

which is always positive that means the pitch restoration moment always increases as the pitch displacement increases.

Yaw

The yaw restore moment is generated by lateral arrays. Supposing the lateral array pairs are in non-equilibrium position with displacement of +Δy for front array 1 and 2, and -Δy for rear array 4 and 5. L_{xla} is the distance between the centers of lateral array to the center of vehicle in x direction. The yaw angle is $\varphi \approx \Delta y / L_{xla}$.

$$\begin{aligned} &F_{1\_unbncd} = F_{5\_unbncd} \\ &= \frac{B_0^2 w^2}{2kL} \frac{1}{1+(R/\omega L)^2} \exp(-2k(y_0+\Delta y)) \\ &\approx 2F_{bncd\_y} \cdot \left[1 - 2kL_{xla}\varphi + 2(kL_{xla})^2\varphi^2\right] \end{aligned} \tag{16}$$

Applying to same equation to the other pair, then we get

$$2F_{bncd\_y} \cdot \left[1 + 2kL_{xla}\varphi + 2(kL_{xla})^2\varphi^2\right]$$

$$T_{yaw\_unbncd} = 8F_{bncd\_y} \cdot L_{xla}{}^2 k\varphi$$

The yaw stiffness

$$\frac{\partial(T_{yaw\_unbncd})}{\partial(\varphi)} = 8F_{bncd\_y} \cdot L_{xla}{}^2 k$$

is always positive, meaning that the yaw restore moment always increases as the yaw displacement increases.

The above analyses and calculations are based on separated pitch angle $\theta = \Delta z / L_x$, the roll angle $\phi = \Delta z / L_y$, yaw angle $\varphi = \Delta y / L_{xla}$, and lateral displacement Δy. These displacements are very small in a real system, and coupling can be neglected in real situations.

3. Optimized Damping Control

For small displacements around the nominal position, the high order terms are negligible compared to the principal terms. The simplified vehicle dynamics are given by [10]

$$\mathbf{M}_{\mathbf{RB}}\ddot{a}_0 = \boldsymbol{\tau}_{\mathbf{RB}} \tag{17}$$

where,

$$\tau_{RB0} = [F_y \quad F_z \quad M_K \quad M_M \quad M_N]^T, a_0 = [\Delta y, \Delta z, \phi, \theta, \varphi]^T$$

$\mathbf{M_{RB}}$ is a positive definite matrix of inertial terms and $\boldsymbol{\tau}_{\mathbf{RB}}$ is the vector that represents all external forces applied to the maglev carriage.

$$\mathbf{M}_{\mathbf{RB}} = \begin{bmatrix} m & 0 & 0 & 0 & 0 \\ 0 & m & 0 & 0 & 0 \\ 0 & 0 & I_{xx} & 0 & 0 \\ 0 & 0 & 0 & I_{yy} & 0 \\ 0 & 0 & 0 & 0 & I_{zz} \end{bmatrix}$$

Substituting the passive Halbach array only forces and moments into Equation (18) with neglecting the high order terms we get equations.

$$\begin{aligned} &\tau_{RB} = \tau_0 \\ &= [-8F_{bncd\_y}k\Delta y \quad -2mgk\Delta z \quad -8F_{bncd\_y}kL_z^2\phi \\ &\quad -0.12F_{bncd\_y}kL_x^2\theta \quad -8F_{bncd\_y}kL_{xlat}^2\varphi]^T \end{aligned} \tag{18}$$

$$\mathbf{M}_{\mathbf{RB}\,0}\ddot{a}_0 = \boldsymbol{\tau}_0 = -K_{st\,0}a_0 \tag{19}$$

where,

$$K_{st0} = \begin{bmatrix} 8F_{bncd\_y}k & 0 & 0 & 0 & 0 \\ 0 & 2mgk & 0 & 0 & 0 \\ 0 & 0 & 8F_{bncd\_y}kL_z^2 & 0 & 0 \\ 0 & 0 & 0 & 0.12F_{bncd\_y}kL_x^2 & 0 \\ 0 & 0 & 0 & 0 & 8F_{bncd\_y}kL_{xlat}{}^2k \end{bmatrix}$$

Δz is the vehicle displacement from equilibrium position in levitation direction, and Δy is the vehicle displacement laterally from equilibrium position. From (19), it is clear that the dynamic modeling has no damping terms. The system equation with control is given by

$$\boldsymbol{M}_{\boldsymbol{RB}0}\ddot{a}_0 + K_{st0}\,a_0 + u = 0 \tag{20}$$

where u is the control input with are give as

$$u = [u_y \; u_z \; u_\phi \; u_\theta \; u_\varphi]$$

Then, control force equations are given as

$$\begin{aligned} u_y &= \sum F_y = K_y \dot{\Delta y}, \qquad u_z = \sum F_z = K_z \dot{\Delta z} \\ u_\phi &= L_y \cdot \sum M_x = K_\phi \dot{\phi}, \quad u_\theta = L_x \cdot \sum M_z = K_\theta \dot{\theta} \\ u_\varphi &= L_{xlat} \cdot \sum M_y = K_\varphi \dot{\varphi} \end{aligned} \tag{21}$$

$K_d = [K_y \;\; K_z \;\; K_\phi \;\; K_\theta \;\; K_\varphi]^T$ is the damping control factors. To solve these equations some constraints can be introduced given the practical situation to get optimized solutions. To minimize the mean square of control forces by (min $\{\sum F^2\}$) can be solved with Lagrange multiplier optimization method.

$$\begin{aligned} Lag = {} & F^2_{z_3} + F^2_{z_1} + F^2_{z_2} + F^2_{z_6} + F^2_{z_5} + F^2_{z_4} \\ & + \lambda_1 (F_{z_3} - F_{z_1} - F_{z_2} + F_{z_6} - F_{z_5} - F_{z_4} - u_z) \\ & + \lambda_2 (F_{z_3} - F_{z_1} - F_{z_2} - F_{z_6} + F_{z_5} + F_{z_4} - \frac{u_\theta}{L_x}) \end{aligned} \tag{22}$$

The solutions are given as.

$$F_{z_3} = -\frac{\lambda_1 + \lambda_2}{2} = -\frac{u_z}{4} - \frac{u_\theta}{4L_x}, F_{z_1} = -\frac{-\lambda_1 - \lambda_2}{2} = \frac{u_z}{4} + \frac{u_\theta}{4L_x}$$

$$F_{z_2} = -\frac{-\lambda_1 - \lambda_2}{2} = \frac{u_z}{4} + \frac{u_\theta}{4L_x}, F_{z_6} = -\frac{\lambda_1 - \lambda_2}{2} = -\frac{u_z}{4} + \frac{u_\theta}{4L_x}$$

$$F_{z_5} = -\frac{-\lambda_1 + \lambda_2}{2} = \frac{u_z}{4} - \frac{u_\theta}{4L_x}, F_{z_4} = -\frac{-\lambda_1 + \lambda_2}{2} = \frac{u_z}{4} - \frac{u_\theta}{4L_x}$$

$$\begin{aligned} Lag = {} & F^2_{y_1} + F^2_{y_2} + F^2_{y_4} + F^2_{y_5} \\ & + \lambda_1 (F_{y_1} - F_{y_2} + F_{y_4} - F_{y_5} - u_y) \\ & + \lambda_2 (F_{y_1} - F_{y_2} + F_{y_4} - F_{y_5} - \frac{u_\phi}{L_y}) \\ & + \lambda_3 (F_{y_1} - F_{y_2} + F_{y_4} - F_{y_5} - \frac{u_\phi}{L_{xLat}}) \end{aligned} \tag{23}$$

The solutions are given as.

$$F_{y_1} = -\frac{\lambda_1 + \lambda_2 + \lambda_3}{2} = -\frac{u_y}{4} - \frac{u_\phi}{4L_y} - \frac{u_\varphi}{4L_{xLat}}$$

$$F_{y_2} = -\frac{-\lambda_1 - \lambda_2 - \lambda_3}{2} = \frac{u_y}{4} + \frac{u_\phi}{4L_y} + \frac{u_\varphi}{4L_{xLat}}$$

$$F_{y_4} = -\frac{\lambda_1 + \lambda_2 + \lambda_3}{2} = -\frac{u_y}{4} - \frac{u_\phi}{4L_y} - \frac{u_\varphi}{4L_{xLat}}$$

$$F_{y_5} = -\frac{-\lambda_1 - \lambda_2 - \lambda_3}{2} = \frac{u_y}{4} + \frac{u_\phi}{4L_y} + \frac{u_\varphi}{4L_{xLat}}$$

4. Optimized LQR Control and Simulation

LQR is a linear optimal control with quadratic performance indices. For system

$$\dot{x} = Ax + Bu \tag{24}$$

where x is a state vector [n × 1], u is the control vector [r × 1], A is a constant matrix [n × n], and B is a constant matrix [n × r][11] .

The performance index is given by

$$J = \int_0^\infty (x^* Q x + u^* R u) dt \tag{25}$$

where x^* is the complex conjugate of the transpose of matrix $\boldsymbol{x}$ and the control vector is given by

$$u(t) = -Kx(t) \tag{26}$$

where Q is the weighting matrix on the states [n×n], R is a positive scalar and yields a matrix of optimal gains K for the state feedback.

The optimization of the cost function gives the optimal control signal u.

$$K = R^{-1} B \times P \tag{27}$$

where $P = P^T$,is the unique positive definite solution of the algebraic Riccati equation

$$A^* P + PA - PBP^{-1} B^* P + Q = 0 \tag{28}$$

The weighting matrix Q =I and R =1 are presented in this paper to demonstrate the effectiveness of the design.

The controller can be designed separately according the LQR optimized control theory. Following we will give the design one by one.

Let define, , $x_{1y} = \Delta Y$, $x_{2y} = \Delta \dot{Y}$, $K_{st0y} = 8F_{bncd\_y} k$.

The lateral system equation is given by

$$\dot{x}_y = A_y x_y + B_y u_y \tag{29}$$

Where

$$\dot{x}_y = [x_{1y} \; x_{2y}] \quad , A_y = \begin{bmatrix} 0 & 1 \\ -\frac{K_{st0y}}{m} & 0 \end{bmatrix}, \quad B_y = \begin{bmatrix} 0 \\ -\frac{1}{m} \end{bmatrix}$$

substituting these into Equation (28), we get equation

$$\begin{aligned} & \begin{bmatrix} -\frac{K_{st0y}}{m} p_{12} & -\frac{K_{st0y}}{m} p_{22} \\ p_{11} & p_{12} \end{bmatrix} + \begin{bmatrix} -\frac{K_{st0y}}{m} p_{12} & p_{11} \\ -\frac{K_{st0y}}{m} p_{22} & p_{12} \end{bmatrix} \\ & - \begin{bmatrix} (\frac{1}{m})^2 p_{12}^2 & (\frac{1}{m})^2 p_{12} p_{22} \\ (\frac{1}{m})^2 p_{12} p_{22} & (\frac{1}{m})^2 p_{22}^2 \end{bmatrix} + \begin{bmatrix} 1 & 0 \\ 0 & 1 \end{bmatrix} = 0 \end{aligned} \tag{30}$$

solving it and select the positive values, the results are given as

$$p_{12} = m(\sqrt{K_{st0y}^2 + 1} - 1)$$
$$p_{11} = (\sqrt{1 + 2m(\sqrt{K_{st0y}^2 + 1} - 1)})((\sqrt{K_{st0y}^2 + 1} - 1) + K_{st0y}) \quad (31)$$
$$p_{22} = m(\sqrt{1 + 2m(\sqrt{K_{st0y}^2 + 1} - 1)})$$

substituting these into (27), we get the optimized control gain matrix K,

$$\begin{aligned} K &= R^{-1} B^* P \\ &= \begin{bmatrix} 0 & \frac{1}{m} \end{bmatrix} \begin{bmatrix} p_{11} & p_{12} \\ p_{12} & p_{22} \end{bmatrix} \\ &= [(\sqrt{K_{st0y}^2 + 1} - 1) \sqrt{1 + 2m(\sqrt{K_{st0y}^2 + 1} - 1)}] \end{aligned} \quad (32)$$

and the optimized control is

$$\begin{aligned} u_y &= Kx \\ &= \left[\sqrt{K_{st0y}{}^2 + 1} - 1 \quad \sqrt{1 + 2m(\sqrt{K_{st0y}{}^2 + 1} - 1)} \right] \left[\Delta Y \, \Delta \dot{Y} \right]^T \\ &= [\sqrt{K_{st0y}{}^2 + 1} - 1] \Delta Y + \sqrt{1 + 2m(\sqrt{K_{st0y}{}^2 + 1} - 1)} \Delta \dot{Y} \end{aligned} \quad (33)$$

Similarly, the optimized control can be derived for $u_z, u_\phi, u_\theta, and\ u_\varphi.$

$$u_z = [\sqrt{K_{st0y}{}^2 + 1} - 1] \Delta Z + \sqrt{1 + 2m(\sqrt{K_{st0y}{}^2 + 1} - 1)} \, \Delta \dot{Z}$$
$$u_\phi = [\sqrt{K_{st0\phi}{}^2 + 1} - 1] \phi + \sqrt{1 + 2I_{xx}(\sqrt{K_{st0\phi}{}^2 + 1} - 1)} \, \dot{\phi}$$
$$u_\theta = [\sqrt{K_{st0\theta}{}^2 + 1} - 1] \theta + \sqrt{1 + 2I_{yy}(\sqrt{K_{st0\theta}{}^2 + 1} - 1)} \, \dot{\theta}$$
$$u_\varphi = [\sqrt{K_{st0\varphi}{}^2 + 1} - 1] \varphi + \sqrt{1 + 2I_{zz}(\sqrt{K_{st0\varphi}{}^2 + 1} - 1)} \, \dot{\varphi}$$

where $K_{st0z} = 2mgk$, $K_{st0\phi} = 8F_{bncd\_y} kL_y{}^2$,
$K_{st0\theta} = 0.12F_{bncd\_y} kL_x{}^2$, and $K_{st0\varphi} = 8F_{bncd\_y} kL_{xlat}{}^2$

With same procedure as the optimized damping control to minimize the mean square of control forces using (22) and (23).

5. SIMULATION

This simulation utilizes the six degrees of freedom model from the Simulink® toolbox. The toolbox model was then modified to use the inertial position, inertial velocity and Euler angles outputs to determine the position of the carriage magnets based on the geometry of the carriage. Limits were then applied to these positions based on the geometry of the track.

Simulation Parameters
The following table summarizes the parameters of the Inductrack system considered for simulation purposes [5]:

Description	Parameter Value
Length of Cradle	65 cm
Cradle Mass (m)	9.3 kg
Volume of Magnet	(1cm x 13cm x 12cm)
Wavelength (λ)	0.1 m
Total length of Halbach Arrays (w)	0.12 m
Resistance / loop (R)	(1.5 x 10^{-3}) Ω
Inductance / loop (L)	(2.6x 10^{-6}) H
Theoretical Surface field (B_0)	0.9 Tesla
K	(2 x π / λ)

Analysis of Results

In figure 3 and 4, the 6DOF vehicle dynamics with a small disturbance is shown under no control and a steady acceleration force. The simulation shows that small disturbance affects system dynamics and the oscillation will not be decayed.

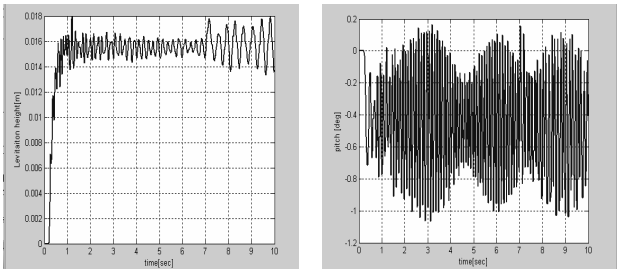

Fig 3. System Response, levitation height and pitch

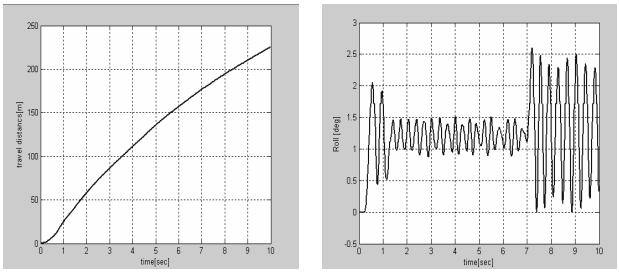

Fig 4. System Response, travel distance and roll

Figure 5 and 6, it shows the system dynamics under optimized damping control, which has the advantage of simple and the requirement for implementation. The result shows oscillation is decreasing levitation height, pitch, roll and lateral position also.

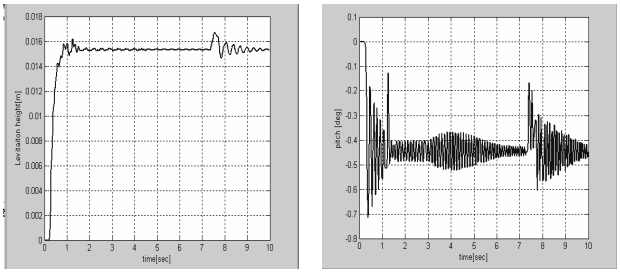

Fig 5. System Response, levitation height and pitch

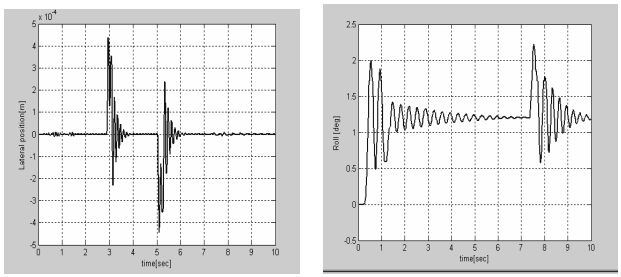

Fig 6. System Response, Lateral position and pitch

Figures 7 and 8 show the system dynamics under the optimized LQR control and comparing to the damping control response, better result is shown in levitation height, pitch and lateral position.

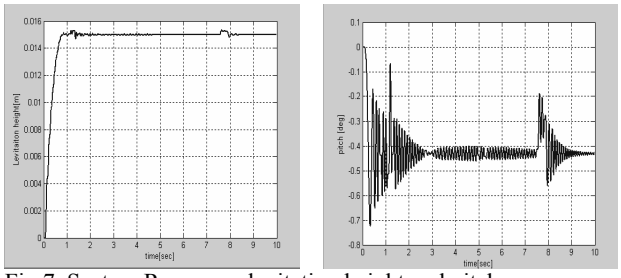

Fig 7. System Response, levitation height and pitch

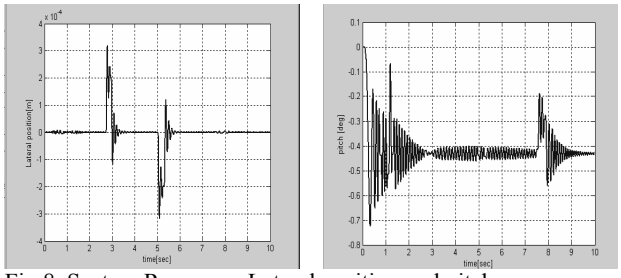

Fig 8. System Response, Lateral position and pitch

6. CONCLUSIONS

In this study, the dynamic motional characteristics of the LLNL Maglev were investigated. The 6 DOF dynamics of the vehicle is complex and inherently unstable. In order to compensate the dynamic instability, an optimized damping and a LQR controls for the vehicle were developed. As showed in the simulation, the proposed control schemes provide the operational stability of the Maglev. The analysis and simulation results will be used as guidance for further theory and experimental research.

7. REFERENCES

[1] William A. Jacobs, PE, "Magnetic Launch Assist NASA's Vision for the Future (May, 2000)", **IEEE Trans. on Magnetics**., Vol. 37, January 2001.

[2] R.F. Post, "**Magnetic Levitation for Moving Objects**," U.S. Patent 5,722,326.

[3] L.S. Tung, R.F. Post, J. Martinez-Frias, **Final Progress Report for the NASA Inductrack Model Rocket Launcher at the Lawrence Livermore National Laboratory**, Livermore California, June 27, 2001

[4] R.F. Post, L.S. Tung, E. Cook, J. Martinez-Frias, The NASA Inductrack Model Rocket Launcher at the Lawrence Livermore National Laboratory, 5th **International Symposium on Magnetic Suspension Technology**, Dec 1999.

[5] R.F. Post, D.D. Ryutov, "**The Inductrack: A Simpler Approach to Magnetic Levitation**," Lawrence Livermore National Laboratory, Livermore, California September 27, 1999.

[6] J. H. Blakelock, **Automatic Control of Aircraft and Missiles**, John Wiley & Sons. 1991.

[7] D. Mcruer, I. Ashkenas, and D. Graham, **Aircraft Dynamics and Automatic Control**, Princeton University Press. 1973.

[8] R.F. Post, "**Inductrack Demonstration Model**," Lawrence Livermore National Laboratory, Livermore, California. February 3, 1998.

[9] R.Kluka, W.Ko, Q.Han, K.Navale, and C.Ham, "Development of a Maglev Vehicle's Control Mechanism for Space Launch", The 8th World Multi-Conference on Systemics, Cybernectics and Informatics SCI 2004, Vol. VIII, Jul 2004

[10] B. V. Jayawant, **Electromagnetic Levitation and Suspension Techniques**, Edward Arnold Ltd. London, 1981.

[11] B. Anderson, and J. Moore, **Optimal control: linear quadratic methods**, Prentice Hall, Englewood Cliffs, New Jersey, 1990.

[12] Qinghua Han, "**Analysis and Modeling the EDS Maglev system based on the Halbach permanent magnet array**," Dissertation, Univ. of Central Florida, summer 2004.